JOURNAL OF AIRCRAFT
Vol. 41, No. 3, May–June 2004

Oscillatory Blowing Control Numerical Simulation of Airfoil Flutter by High-Accuracy Method

Jin Yan* and Yuan Xin†
Tsinghua University, 100084 Beijing, People's Republic of China

It is known that oscillatory blowing can be used to delay flow separation and stall. The oscillatory blowing technique is applied to control of the airfoil's flutter. A high accuracy fluid–structure coupling numerical method is used. The numerical results show that the steady blowing will weaken the flutter. However, the excess blowing will decrease the lift coefficient. The best blowing velocity can be found by the present numerical method. The influence of the frequency of the oscillatory blowing on the airfoil's vibration is also studied. The numerical results show that the oscillatory blowing is more efficient than steady blowing.

Introduction

WHEN a freestream flows past an airfoil at large incidence angle, an unsteady vertical structure will be generated near the airfoil. The unsteady lift and pitching moments may lead to airfoil flutter. When the energy transformed from the airstream to the airfoil is positive and increases with time, structure oscillation will grow rapidly, and the system becomes unstable, which is called stall flutter. Flutter, especially stall flutter, will be harmful to the safety and efficiency of the aircraft devices. Flutter will also cause noise pollution. Thus, the control of flutter or at least its mitigation is always considered in engineering applications.

Flutter at large incidence angle is often related to boundary-layer separation. Many techniques have been used in aeronautics to delay separation, such as modification of geometrical shaping, turbulators, and passive transpiration. Experiments performed at low Renolds and Mach numbers (Refs. 1–4) have shown that cyclic vertical oscillations introduced into a separation boundary layer slightly upstream of the average separation location can effectively delay boundary-layer separation. The improved ability of the boundary layer to overcome an adverse pressure gradient is attributed to enhanced mixing between the low-momentum fluid near the wall and the external high-momentum flow. This process becomes extremely efficient if the forcing frequencies correspond to the most unstable frequencies of the separating shear layer. The delay of boundary-layer separation increases the airfoil maximum lift, while maintaining low drag. From the experimental results, it is shown that oscillatory blowing is significantly more effective than steady blowing.[2,4] Seifert et al.[1] and Seifert and Pack[2] have drawn the conclusion that oscillatory blowing can delay boundary-layer separation, and the reduced frequencies in the range 0.5–1 is the most effective.

The purpose of the present paper is to apply the oscillatory blowing technique to control the airfoil flutter. A fluid–structure coupling numerical method is used. The Favre-averaged Navier–Stokes equations and a low Reynolds number q–ω turbulence model[5] have been adopted to serve as the governing equation for the fluid zone. A pitch and a plunge airfoil (PAPA) model is employed in the structure. A higher-order, high resolution MUSCL total variational diminishing (TVD) scheme[8] and an implicit lower–upper symmetric Gauss–Seidel (LU-SGS-GE) scheme (see Ref. 7), have been used to calculate the flowfield and can accurately simulate the unsteady large-scale vortex. The fourth-order Runge–Kutta method has been used to solve the oscillation equations in the solid zone. Boundary conditions are transferred between the two zones after each time step. A case of deep dynamic stall is calculated to validate the code. Following the code validation, the present techniques are employed to analyze flutter problems at large incidence angles ($10 \sim 50$ deg) and blowing control technique. The influence of oscillatory blowing on the airfoil's vibration is studied.

Mathematical Formulation

The governing equations of turbulence flow fluid and structure are presented in this section. All of the variables in the equations are nondimensional. The characteristic length is c. The characteristic velocity is a_∞.

Governing Equations of Fluid

The Favre-averaged, two-dimensional, Navier–Stokes equations can be written in body-conforming curvilinear coordinate system as follows:

$$\frac{\partial \hat{Q}}{\partial t} + \frac{\partial \hat{F}_i}{\partial \xi_i} + \frac{1}{Re}\hat{D} + \hat{S} = 0 \tag{1}$$

$$\hat{Q} = J\begin{bmatrix} \rho \\ \rho u_1 \\ \rho u_2 \\ \rho u_3 \\ \rho E \\ \rho \vartheta_1 \\ \rho \vartheta_2 \end{bmatrix}, \qquad \hat{F}_i = J\begin{bmatrix} \rho U_i \\ \rho u_1 U_i + \xi_{i,1} p \\ \rho u_2 U_i + \xi_{i,2} p \\ \rho u_3 U_i + \xi_{i,3} p \\ \rho H U_i - \xi_{i,t} p \\ \rho \vartheta_1 U_i \\ \rho \vartheta_2 U_i \end{bmatrix}$$

$$\hat{D} = \frac{\partial}{\partial \xi_i} J \xi_{i,j} \begin{bmatrix} 0 \\ \tau_{j1} \\ \tau_{j2} \\ \tau_{j3} \\ \tau_{jl} u_l + \varpi_j(k) - q_j \\ \varpi_j(\vartheta_1) \\ \varpi_j(\vartheta_2) \end{bmatrix}, \qquad \hat{S} = -J\begin{bmatrix} 0 \\ 0 \\ 0 \\ 0 \\ 0 \\ S_{\vartheta_1} \\ S_{\vartheta_2} \end{bmatrix} \tag{2}$$

where t is the nondimensional time, ρ is the density, u_i is the velocity component, $\xi_{i,j} = \partial \xi_i / \partial x_j$, $\xi_{i,t} = \partial \xi_i / \partial t$, $J = \partial(x_1, x_2)/\partial(\varsigma_1, \xi_2)$, and $U_i = \xi_{i,j} + \xi_{i,t}$ is the contravariant velocity component. $E = e + u_l u_l/2 + k$ and $H = h + u_l u_l/2 + k$ are the, stagnation energy and the stagnation enthalpy, respectively, e and h are the energy and enthalpy, k is the turbulence kinetic energy, pressure p is expressed by the general gas law, τ_{ij} is the sum of the molecular and

Received 3 February 2003; revision received 12 February 2003; accepted for publication 31 March 2003.

*Ph.D. Student, Department of Thermal Engineering; Jinyan99@mails.tsinghua.edu.cn.

†Professor, Department of Thermal Engineering; yuanxin@mail.tsinghua.edu.cn.

the Renolds stress tensor, and $\boldsymbol{q}_i$ is the total of the molecular and turbulence heat flow vector:

$$\tau_{ij} = (\mu + \mu_t)\left(\frac{\partial u_i}{\partial x_j} + \frac{\partial u_j}{\partial x_i} - \frac{2}{3}\delta_{ij}\frac{\partial u_l}{\partial x_l}\right) - \frac{2}{3}\delta_{ij}\rho k Re \quad (3)$$

$$\boldsymbol{q}_i = -\left(\frac{\mu}{Pr} + \frac{\mu_t}{Pr_t}\right)\frac{\partial h}{\partial x_i} \quad (4)$$

$$\varpi_i(\vartheta_m) = \left(\mu + \frac{\mu_t}{Pr_{\vartheta_m}}\right)\frac{\partial \vartheta_m}{\partial x_i} \quad (5)$$

where Re is the Renolds number and Pr and Pr_t are the laminar and turbulence Prandtl numbers respectively. Here μ is the molecular viscosity, and turbulence viscosity μ_t is determined by the additional variable ϑ_1 and ϑ_2, where $\mu_t = \mu_t(\vartheta_1, \vartheta_2)$.

JU_i can also be chosen as the volume flux in the governing equations of body-conforming curvilinear coordinate system. The new equations can be derived from Eq. (1) with a matrix of linear transformation B:

$$B\left[\frac{\partial \hat{Q}}{\partial t} + \frac{\partial \hat{F}_i}{\partial \xi_i} + \frac{1}{Re}\hat{D} + \hat{S}\right] = \frac{\partial \tilde{Q}}{\partial t} + \frac{\partial \tilde{F}_i}{\partial \xi_i} + \tilde{\boldsymbol{R}} + \frac{1}{Re}\tilde{D} + \tilde{S} = 0 \quad (6)$$

$$\tilde{Q} = J\begin{bmatrix}\rho\\ \rho U_1\\ \rho U_2\\ \rho U_3\\ \rho E\\ \rho\vartheta_1\\ \rho\vartheta_2\end{bmatrix}, \qquad \tilde{F}_i = J\begin{bmatrix}\rho U_i\\ \rho U_1 U_i + \xi_{i,1}p\\ \rho U_2 U_i + \xi_{i,2}p\\ \rho U_3 U_i + \xi_{i,3}p\\ \rho H U_i\\ \rho\vartheta_1 U_i\\ \rho\vartheta_1 U_i\end{bmatrix}$$

$$B = \begin{bmatrix}1 & 0 & 0 & 0 & 0 & 0 & 0\\ 0 & \xi_{1,1} & \xi_{1,2} & \xi_{1,3} & 0 & 0 & 0\\ 0 & \xi_{2,1} & \xi_{2,2} & \xi_{2,3} & 0 & 0 & 0\\ 0 & \xi_{3,1} & \xi_{3,2} & \xi_{3,3} & 0 & 0 & 0\\ 0 & 0 & 0 & 0 & 1 & 0 & 0\\ 0 & 0 & 0 & 0 & 0 & 1 & 0\\ 0 & 0 & 0 & 0 & 0 & 0 & 1\end{bmatrix} \quad (7)$$

where $g_{ij} = \xi_{i,l}\xi_{j,l}$ and $\tilde{\boldsymbol{R}}$ is an additional vector.

Turbulence Model

Selecting an appropriate turbulence model is important to simulate accurately the unsteady flowfield of an oscillating airfoil. In the past 20 years, two-equation turbulence models that are based on the hypothesis of eddy viscosity were developed because they can be used to simulate complicated vortical structures and are simple enough for engineering applications. Compared with other two-equation models, the q–ω turbulence model[5] has the unique advantages of lower computational cost, good adaptation to coarse turbulence, and more easily treated boundary conditions.

The equations of the q–ω model can be given as follows:

$$\mu_t = ReC_\mu f_\mu(\rho q^2/\omega), \qquad \vartheta_1 = q = \sqrt{k}, \qquad \vartheta_2 = \omega = \varepsilon/k$$

$$S_q = \tfrac{1}{2}\left[C_\mu f_\mu(J/\omega^2) - \tfrac{2}{3}(\Phi/\omega) - 1\right]\rho\omega q$$

$$S_\omega = \left\{C_1 f_1\left[C_\mu(J/\omega^2) - C_3(\Phi/\omega)\right] - C_2\right\}\rho\omega^2$$

$$f_\mu = 1 - \exp(-0.02Re_t), \qquad f_1 = 1 + 9f_\mu$$

$$Re_t = Re(\rho q l_w/\mu), \qquad C_\mu = 0.09, \qquad C_1 = 0.05$$

$$C_2 = 0.83, \qquad C_3 = 0.6, \qquad Pr_q = 0.8, \qquad Pr_\omega = 2.0 \quad (8)$$

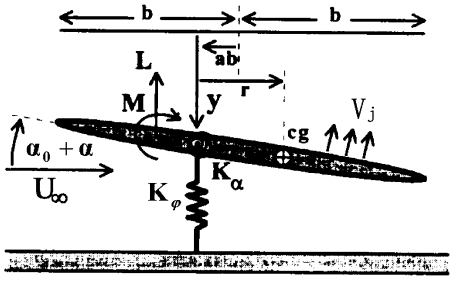

Fig. 1 Schematic diagram of the PAPA model.

Equations of Structure

The structural dynamics model considered is the PAPA model, as shown in Fig. 1. The airfoil degrees of freedom are the pitch angle α, positive nose up, and plunge displacement φ. The governing equations for the structure are

$$M\ddot{Y} + D\dot{Y} + KY + S = F \quad (9)$$

$$Y = \begin{bmatrix}\varphi\\ \alpha\end{bmatrix}, \qquad M = \begin{bmatrix}1 & S_\alpha\cos(\alpha_0+\alpha)\\ S_\alpha\cos(\alpha_0+\alpha) & I_\alpha\end{bmatrix}$$

$$K = \begin{bmatrix}\dfrac{4\omega_\varphi^2 M_\infty}{U^{*2}\omega_\alpha^2} & 0\\ 0 & \dfrac{4\omega_\alpha^2 M_\infty}{U^{*2}\omega_\alpha^2}\end{bmatrix}$$

$$D = \begin{bmatrix}\dfrac{4\varsigma_\varphi\omega_\varphi M_\infty}{U^*\omega_\alpha} & 0\\ 0 & \dfrac{4\varsigma_\alpha\omega_\alpha M_\infty}{U^*}\end{bmatrix}$$

$$S = \begin{bmatrix}-S_\alpha\sin(\alpha_0+\alpha)\dot{\alpha}^2\\ 0\end{bmatrix}, \qquad F = \begin{bmatrix}-\dfrac{2M_\infty^2 C_l}{\pi\mu'}\\ \dfrac{2M_\infty^2 C_m}{\pi\mu'}\end{bmatrix} \quad (10)$$

where α_0 is the static incidence angle, S_α and I_α are the static moment and the rotational moment of the airfoil, C_l is the lift coefficient, C_m is the moment coefficient, ς_α and ς_φ are the damping coefficients, $U^* = 2U_\infty/(c\omega_\alpha)$, U_∞ is the freestream velocity, M_∞ is the freestream Mach number, ω_α and ω_φ are the natural frequencies, and μ' is the mass ratio.

Numerical Scheme

A loose fluid–structure coupling approach has been applied to analyze the flutter of airfoils. The fluid and solid variables are updated alternatively by independent computational fluid dynamics and computational structural dynamics codes which exchange boundary information at each time step.

An implicit time-marching scheme is used to compute the unsteady Navier–Stokes equations. When a second-order Crank–Nicholson method and Newton subiteration are applied to Eq. (6), a δ-type implicit equation can be obtained as follows:

$$\left(I + \theta\Delta t\frac{\partial}{\partial\xi_i}\tilde{A}_i^n\right)\delta\tilde{Q}^{(m)} = -\left(\tilde{Q}^{(m)} - \tilde{Q}^n\right) + \frac{1}{2}\left(\tilde{R}^n + \tilde{R}^{(m)}\right) \quad (11)$$

$$\tilde{Q}^{(m+1)} = \tilde{Q}^{(m)} + \delta\tilde{Q}^{(m)}, \qquad \tilde{Q}^{(0)} = \tilde{Q}^n, \qquad 0 \le \theta \le 1$$

$$\tilde{A} = \frac{\partial\tilde{F}_i}{\partial\tilde{Q}}, \qquad \tilde{R} = -\Delta t B\left(\frac{\partial\hat{F}_i}{\partial\xi_i} + \frac{1}{Re}\hat{D} + \hat{S}\right) \quad (12)$$

A new implicit LU-SGS scheme (see Ref. 7) has been used to solve the left-hand side of Eq. (8), which not only contains all of the features of the LU-SGS scheme, but also displays distinctive advantages. Although similarity transformations are used to construct

upwind Jacobian matrix of the flux vectors, the block-diagonal matrix inversions are still eliminated, and the left-hand-side operator can be completely vectorized, too. Because the true Jacobian matrix has been used, the new implicit scheme leads to a much faster convergence and higher stabilization without improper numerical dissipation and free parameters.

A fourth-order MUSCL TVD scheme[8] is used to solve the left-hand side of Eq. (8), which has a higher accuracy, higher resolution, and better stability. It is suitable for solving unsteady flows and capturing the complicated vortex-shedding process.

Body-fitted C-type computational grids, whose meshes modify their positions with time, are generated with a geometry method. The size of the grids is 361×76. A fourth-order Runge–Kutta method is applied to solve equations of the structure.

Results and Discussion

Validation of the Numerical Method

A case of deep dynamic stall was first calculated to validate the code. The specific parameters of dynamic stall are from Ref. 6, $M_\infty = 0.29$ and $Re = 1.95 \times 10^6$. The relationship between incidence angle α_t and nondimensional time t (based on chord c and U_∞) can be expressed as $\alpha(t) = \alpha_0 + \alpha_1 \sin(2kt)$. The amplitude of the incidence angle $\alpha_1 = 4.2$ deg, and the reduced frequency $k = 0.1$. The mean incidence angle is 15 deg. The numerical results agree fairly well with the experimental data of Piziali (see Ref. 6). The detailed numerical results are given in Ref. 9. The lift coefficient hysteresis is shown in Fig. 2.

A case of unsteady oscillatory blowing is simulated, and the numerical results are compared with Seifert and Pack's experimental data,[2] $M_\infty = 0.3$ and $Re = 31.3 \times 10^6$. The airfoil is fixed. The oscillatory blowing is located on the upper surface at 10% chord. The slot is 0.2% chord wide. The oscillatory blowing velocity $V_j = 45 + 25 \sin(260 \times t)$ m/s. The calculated lift coefficient near the static stall angle is calculated by the present numerical method, shown in Fig. 3. The maximum value of C_l as increased by the oscillatory blowing. The numerical results agree fairly well with the experimental data.

The sensitivity of mesh size and time step were studied during the calculation of the unsteady flowfield. It was found that the present

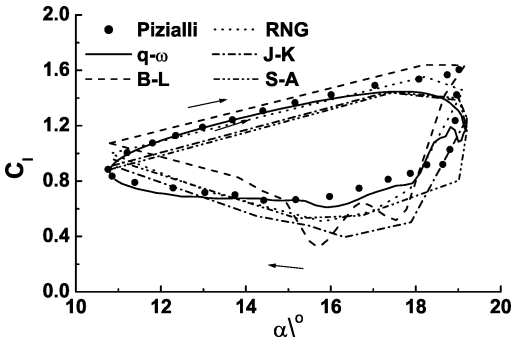

Fig. 2 Lift coefficient hysteresis, $\alpha_0 = 15$ deg.

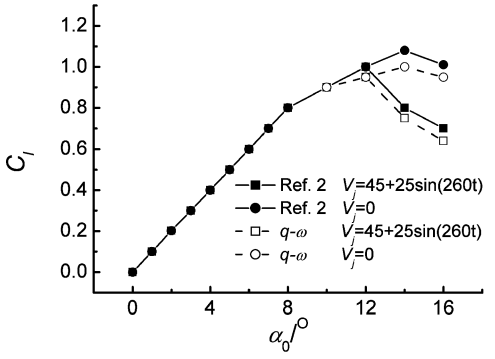

Fig. 3 Unsteady numerical results of oscillatory blowing on NACA 0015 airfoil.

Table 1 Nondimensional structural parameters and aerodynamic parameters

Parameter	Case 1, NACA 0015	Case 2, S809	Case 3, NACA 0015
S_α	0.2	0.2	0.2
I_α	0.3	0.3	0.3
ω_α	0.05	0.05	0.05
ω_φ	0.05	0.05	0.075
$\omega_\varphi/\omega_\alpha$	1	1	1.5
ς_α	0.01	0	0
ς_φ	0.01	0	0
U^*	1.83	0.4636	1.22
Re	1.95×10^6	5×10^5	1.3×10^6
M_∞	0.3	0.076	0.2

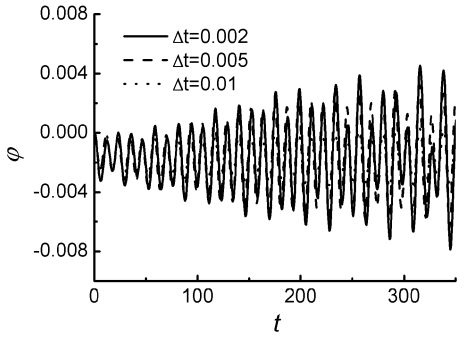

Fig. 4 Influence of time step on the numerical results.

mesh (361×71) is large enough and that the calculation results are independent of the mesh. The same mesh is used in the aeroelastic calculation. It is also found that more than 5000 time steps in a vibration cycle should be used to make the numerical results independent of time step.

In the aeroelastic calculation, the natural frequencies ω_α and ω_φ are used to calculate the cycle of vibration because the vibration around the natural frequencies is most important to stall flutter. Figure 4 shows the influence of time step on the numerical results. When the time step Δt is less than 0.005, the numerical results are similar, although there is still a small difference in the value of the amplitude, which is less important when stall flutter's characteristics are studied. Thus, the time step $\Delta t = 0.005$ is used throughout the aeroelastic calculation.

Analysis of the Flutter and Blowing Control Technique

The airfoil's flutter at large incidence angle, $\alpha_0 = 10 \sim 50$ deg, and blowing control are analyzed by numerical method. The test cases include a NACA 0015 airfoil and an S809 airfoil. The structural parameters and aerodynamic parameters are listed in Table 1.

An unsteady vortical structure can be generated near the suction surface of the airfoil periodically at large attack angle. Figure 5 shows the instantaneous flowfield of case 1 when mean incidence angle $\alpha_0 = 50$ deg. It can be found that the vortex originates alternatively from the leading edge and trailing edge of the airfoil, which can lead to the vibration of the airfoil. The solid line of Fig. 6 is the evolution of α in this case, where α fluctuates between -0.015 and 0.0075 rad. Sometimes the amplitude of flutter caused by the unsteady vortex can be very large, which is harmful to the performance of the airfoil. Here we aim to control the flutter by blowing. The position of blowing is shown in Fig. 1 ($50\%c \sim 80\%c$). The velocity of blowing V_j can be defined as follows: $V_j = V_0 + V_\alpha \sin(2\pi\omega_j t)$, where V_0 is the steady blowing velocity, V_α is the oscillatory blowing velocity, and ω_j is the oscillatory blowing frequency. The dotted line in Fig. 6 is the evolution of α with steady blowing, $V_\alpha = 0$. It is evident that the oscillation can be weakened efficiently by steady blowing. On one hand, the amplitude oscillation decreased with the value of V_j. On the other hand, steady blowing also has strong influence on the lift coefficient C_l of the airfoil. Figure 7 shows the evolution of C_l. When the blowing velocity is appropriate, the average value of C_l will also increase accordingly. For example, when

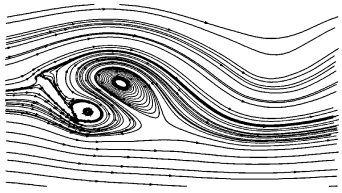

a) $t = 150$

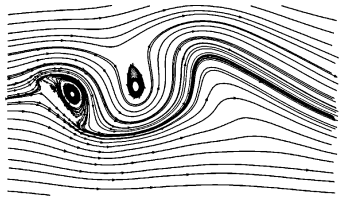

b) $t = 156$

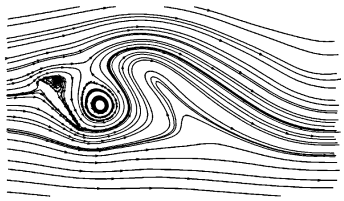

c) $t = 162$

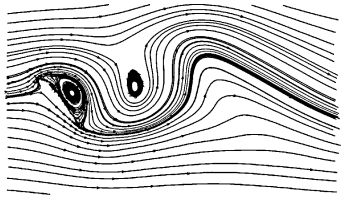

d) $t = 168$

Fig. 5 Evolution of vortex at large mean incidence angle, case 1, $\alpha_0 = 50$ deg.

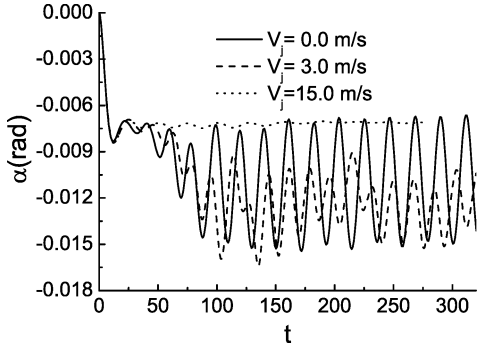

Fig. 6 Evolution of α with $\alpha_0 = 50$ deg.

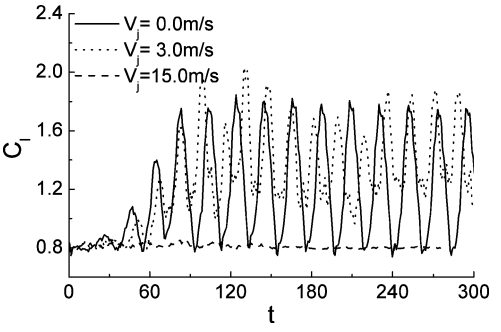

Fig. 7 Evolution of lift coefficient, $\alpha_0 = 50$ deg.

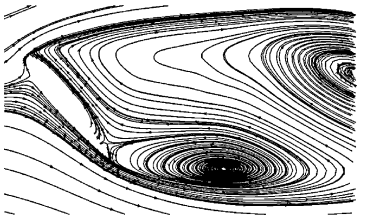

a) $V_j = 3$ m/s

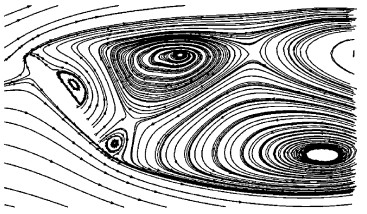

b) =15 m/s

Fig. 8 Influence of blowing on the flow Field, $\alpha_0 = 50$ deg.

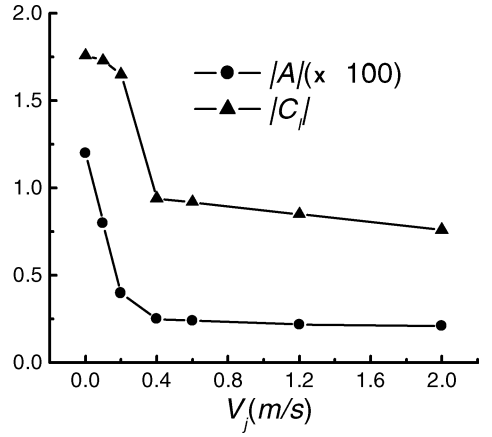

Fig. 9 Influence of V_0 on the oscillation amplitude and lift coefficient (case 1).

$V_j = 3$ m/s, the lift coefficient will fluctuate between 1.2 and 1.75, compared with lift coefficient without blowing, which fluctuates between 0.8 and 1.75. Thus, appropriate steady blowing can improve the performance of the airfoil. However, if the blowing velocity is too large, despite the benefit of decreasing the amplitude of the airfoil's vibration, the average value of the lift coefficient will also drop dramatically. It can be seen in Fig. 7, in the case of $V_j = 15$ m/s, that the lift coefficient is nearly steady, $C_l = 0.8$, which is much lower than the average lift coefficient without blowing.

Figure 8 shows the influence of blowing on the flowfield. When the blowing velocity is appropriate, the blowing fluid will flow along the suction surface of the airfoil, which can reduce the influence of the unsteady main vortex (Fig. 8a). The oscillation will be weakened, and C_l will be increased accordingly. However, if extra blowing is introduced, although the influence of the main vortex upon the flutter is very small, a new vortex is generated along the suction surface (Fig. 8b), which makes C_l drop. Therefore, there is an optimal value of blowing velocity V_j^*, which can be found by the present numerical method.

The influences of blowing velocity on the oscillation amplitude and of the lift coefficient are shown in Figs. 9 and 10. Here, $|\alpha|$ is the average value of α oscillation amplitude, and $|C_l|$ is the average lift coefficient. C_l has a peak value with steady blowing velocity $V_0 = 3$ m/s. In addition, the average oscillation amplitude of α decreases most rapidly when $V_0 = 0 \sim 4$ m/s. Thus, we can determine that the optimal blowing velocity $V_j^* = 3 \sim 4$ m/s.

The similar results are obtained in the case of low-velocity flow (case 2). Figures 11 and 12 show the numerical results of case 2 at the attack angle of 30 deg. The oscillation is divergent without

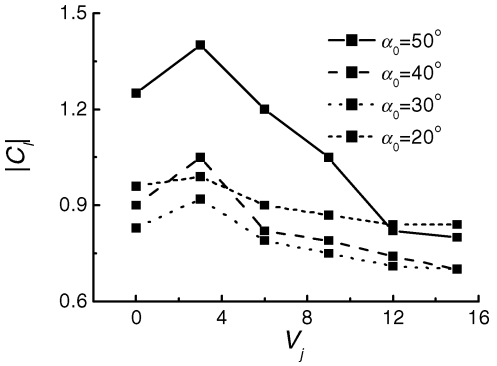

Fig. 10 Influence of ω_j on the oscillation amplitude and lift coefficient (case 1).

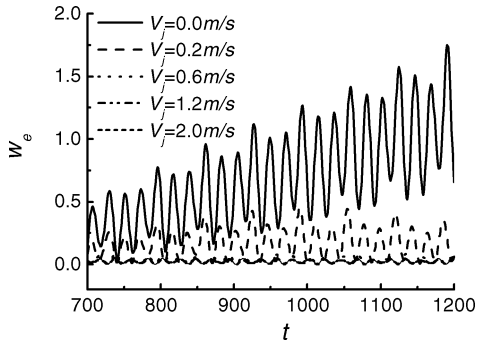

Fig. 11 Evolution of W_e ($\alpha_0 = 30$ deg, case 2).

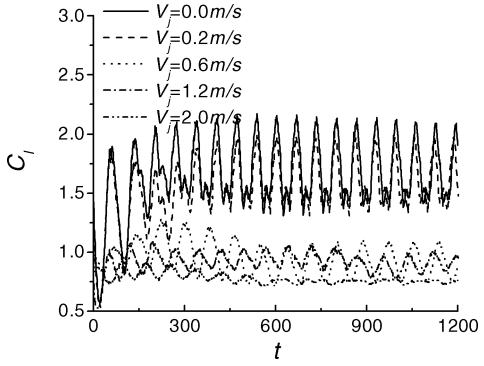

Fig. 12 Evolution of C_l ($\alpha_0 = 30$ deg, case 2).

blowing control. Steady blowing can efficiently make the oscillation stable. Meanwhile, the lift coefficient will also decrease. The amplitude of oscillation drops very quickly when $V_0 = 0 \sim 0.2$ m/s, and the average lift coefficient C_l almost remains the constant when $V_0 = 0 \sim 0.3$ m/s (Fig. 13). The appropriate blowing velocity is $V_j^* = 0.2 \sim 0.3$ m/s.

V_j^* is related to the freestream velocity V_∞. It is found from the numerical results that $V_j^* = 0.01 \sim 0.03 V_\infty$ in general.

The steady blowing is enough to weaken the oscillation in most cases, but it is not always effective when the freestream velocity is high and the structural damping coefficient is small, especially in the case of stall flutter. Steady blowing and oscillatory blowing are compared in a case of stall flutter (Fig. 14). It is found from the numerical results that oscillatory blowing is more efficient than steady blowing. Figure 15 shows the influence of the oscillatory frequency ω_j on the flutter. The oscillation will be aggravated if the frequency of the oscillation is similar to the natural frequencies, ω_α and ω_φ. Furthermore, the oscillatory frequency is more efficient if large ω_j is selected. Therefore, large ω_j (much higher than the natural frequency of the airfoil) is used in the numerical simulation.

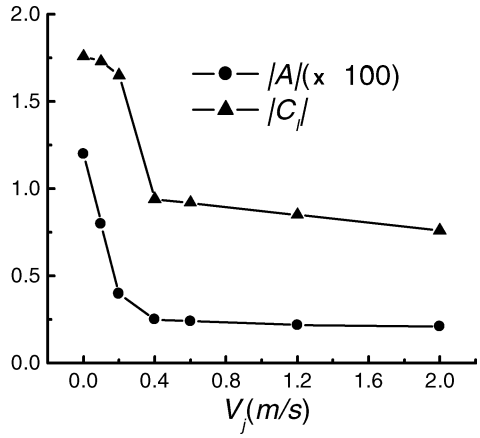

Fig. 13 Influence of V_0 to the oscillation amplitude and lift coefficient, $\alpha_0 = 30$ deg, case 2.

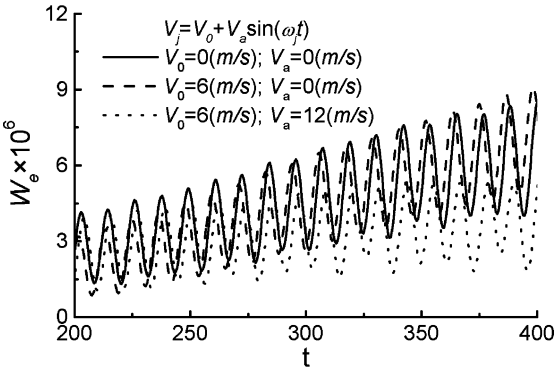

Fig. 14 Evolution of W_e, case 3 $\alpha_0 = 30$ deg and $\omega_j = 0.2$.

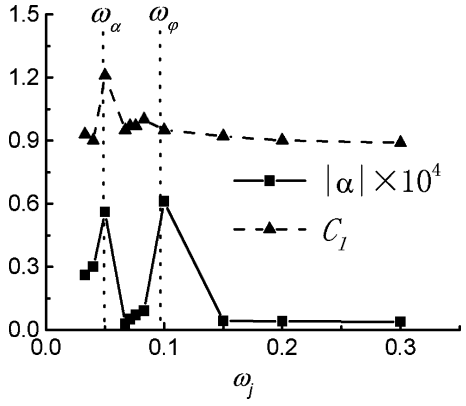

Fig. 15 Influence of ω_j on the oscillation amplitude and lift coefficient, case 3, $\alpha_0 = 30$ deg and $V_j = 3 + 6\sin(2\pi\omega_j t)$.

Conclusions

A high-accuracy fluid–structural coupling numerical method is developed to analyze the blowing control of the airfoil's flutter at large incidence angle (15–60 deg). The numerical results show that the steady blowing will weaken the flutter, but at the same time overblowing will cause the lift coefficient to drop. The optimal blowing velocity V_j^* can be obtained by use of this numerical method, and it is found that $V_j^* = 0.01 \sim 0.03 V_\infty$, in general. Oscillatory blowing is more efficient than steady blowing in the cases of severe flutter. Large oscillatory blowing frequency is more efficient in reducing the airfoil's flutter.

Acknowledgments

The paper is subsidized by the National Natural Science Foundation of the People's Republic of China (Grant 1999022306) and

the Special Funds for Major State Basic Research Projects (Grant 5007609).

References

[1]Seifert, A. Bachar, T., Koss, D., Shepshelovich, M., and Wygnanski, I., "Oscillatory Blowing, a Tool to Delay Boundary Layer Separation," *AIAA Journal*, Vol. 31, No. 11, 1994, pp. 2052–2060; also AIAA Paper 93-0440, 1993.

[2]Seifert, A., and Pack, L. G., "Oscillator Control of Separation at High Reynolds Numbers," *AIAA Journal*, Vol. 37, No. 9, 1999, pp. 1062–1071; also AIAA Paper 98-0214, 1998.

[3]Seifert, A., Daraby, A., Nishri, B., and Wyganski, I., "The Effects of Forced Oscillations on the Performance of Airfoils," AIAA Paper 93-3264, July 1993.

[4]Darabi, A., "Delay Airfoil Stall by Periodic Excitation," *Journal of Aircraft*, Vol. 33, No. 4, 1996, pp. 691–699.

[5]Coakley, T. J., "Turbulence Modeling Methods for the Compressible Navier–Stokes Equations," AIAA Paper 83-1693, 1983.

[6]Daiguji, H., Yuan, X., and Yamamoto, S., "Stabilization of Higher-Order High Resolution Schemes for the Compressible Navier–Stokes Equations," *International Journal for Numerical Methods for Heat and Fluid Flow*, Vol. 7, No. 2, 3, 1997, pp. 250–274.

[7]Yuan, X., and Daiguji, H., "A Specially Combined Lower–Upper Factored Implicit Scheme for Three-Dimensional Compressible Navier–Stokes Equations," *Computers and Fluids*, Vol. 30, No. 3, 2001, pp. 339–363.

[8]Piziali, R. A., "An Experimental Investigation of 2D and 3D Oscillating Wing Aerodynamics for a Range of Angle of Attack Including Stall," NASA TM 4623, 1993.

[9]Jin, Y., and Yuan, X., "Numerical Study of Unsteady Viscous Flow Past Oscillation Airfoil," *Wind Engineering*, Vol. 25, No. 4, 2001, pp. 227–237.